European Journal of Applied Sciences – Vol. 9, No. 4
Publication Date: August 25, 2021
DOI:10.14738/aivp.94.10779.
Kuo, S. P. (2021). Air Plasma Mitigation of Shock Wave. European Journal of Applied Sciences, 9(4). 228-244.

SOCIETY FOR SCIENCE AND EDUCATION

Air Plasma Mitigation of Shock Wave

Spencer P. Kuo
Department of Electrical & Computer Engineering,
New York University-Tandon School of Engineering, Brooklyn, NY, USA

ABSTRACT

Theory is presented to show that shock wave structure can be modified via interacting with an air plasma plume generated symmetrically in front of a shock wave generator. Electron jet in the plasma plume deflects the impinging airflow via momentum transfer collisions. Symmetrical deflection makes it easy to satisfy the conservation of transverse momentum between the airflow and plasma. The charge transfer between N_2^+ and N_2 randomizes the impinging airflow to increase the deflection angle. The flow deflection increases the effective cone angle of the shock generator; as the effective cone angle exceeds a critical value, the shock becomes detached and faded. Experiments were conducted in a Mach 2.5 wind tunnel to mitigate shock wave via air plasma deflection. A non-thermal air plasma was symmetrically generated, in front of a wind tunnel model by on-board 60 Hz periodic electric arc discharge, as a deflector for shock wave mitigation. The results show a transformation of the shock from a well-defined attached shock into a highly curved shock structure, which has increased shock angle and appears in diffused form. Shown in a sequence with increasing discharge intensity, the transformed curve shock in front of the model moves upstream to become detached with increasing standoff distance from the model and is eliminated when the discharge is near the peak. The steady of the incoming flow during the discharge cycle is manifested by the repetition of the baseline shock front. The experimental observations confirm the theory and efficacy of this air plasma mitigator.

Keywords: Shock Wave Mitigation; Air Plasma Deflector; Shadowgraph; Drag Reduction; Wind Tunnel; Electric Discharge.

INTRODUCTION

Shock wave appears in the form of a steep pressure gradient. It introduces a discontinuity in the flow properties at the shock front location. The background pressure behind the shock front increases considerably, leading to significant enhancement of the flow drag and friction on the spacecraft. Thus, the design for supersonic aircraft tends to choose slender shapes to reduce the drag and cooling requirements. This is an engineering tradeoff between volumetric and fuel consumption efficiencies and this tradeoff significantly increases the operating cost of commercial supersonic aircraft. Shock wave also produces sonic booms. The noise issue raises environmental concerns, which have precluded routine commercial supersonic flight over land. There are considerable theoretical and experimental studies comprehend shock waves in super-sonic flows [1] and various approaches to reduce shock wave drag to a supersonic spacecraft have been explored. A physical spike [2] is currently used to move shock wave upstream from the spacecraft. It improves the aspect ratio of a blunt body to reduce shock wave drag. Further mitigation of shock wave impact, shock wave formation around a supersonic

spacecraft must be attenuated or even eliminated. It has the payoff that the fuel consumption is reduced, and smaller propulsion system can provide the same cruise speed.

Thermal energy deposition in front of a flying body to perturb the incoming flow and shock wave formation has been studied [3]-[7]. Heating of the background air in front of a flying body essentially reduces the Mach number of the impinging airflow to the body. As a result, the formed shock is weakened and has an increased shock angle (i.e., moving the shock front upstream). This approach must elevate the gas temperature significantly to effectively reduce the wave drag and shock noise. However, the energy gain from drag reduction is not enough to make up the injected heating energy [5]. Although this is not a practical approach for drag reduction purposes, it can be a feasible approach for sonic boom attenuation [3].

Shock-tube experiments showed the impact of non-thermal plasma on the shock wave structures. Several wind tunnel experiments further explored the non-thermal (and non-equilibrium) plasma effects on shock wave mitigation. In the wind tunnel experiment conducted by Gordeev *et al*. [8], a high Z conducting wire, inside the chamber of a cone-cylinder model, was exploded off electrical short circuit; a high-pressure metal vapor (high Z) plasma was produced and injected into the upstream supersonic flow through a nozzle. A significant drag reduction, which was too large to be accounted for by the thermal effect alone, was measured. In the subsequent wind tunnel experiments [9]-[17], electric discharges were applied to generate plasmas in the supersonic flows to interact with the shock waves. The results showed that the shock front increased dispersion in its structure and/or the standoff distance from the model when the plasma was generated either off-board or on-board ahead of a model. Computational and experimental studies [18] indicated that an added magnetic field could strengthen the arc plasma to further weaken the shock wave. Microwave discharge is another way to generate non-thermal plasma, so far, the microwave plasma projected on-board was still too weak to introduce any visible effect on the shock wave in a hypersonic flow [19].

Theory shows that the shock wave angle and the shock structure depend on the cone angle of the wind tunnel model, and on the Mach number and the deflection angle of the incoming flow [1]. In the present study, the cone angle of the wind tunnel model and the Mach number of the incoming flow are fixed, an on-board plasma deflector is introduced to study shock structure modification by the flow deflection [20]. The polarity of the applied voltage enables electron plasma to be accelerated in the upstream direction by the applied electric field, it forms a plasma deflector in the upstream region to deflect incoming flow through elastic collisions. Ion plasma also affects the incoming flow, but via a different (non-equilibrium) process. Ions moving through their own gas are subject to charge transfer to the neutral gas, which is a predominant inelastic collision process in the low ion energy regime [21]. An ion becomes a neutral particle after the charge transfer, but retains its velocity, which is typically low. Thus, these particles do not contribute to the shock wave formation. The ions converted from neutrals through charge-transfer are collected by the cathode and do not contribute to the shock wave generation either. The shock of the deflected flow is expected to have a larger shock angle (than that of the baseline one) and a modified structure, representing a weaker shock.

In Section 2, Taylor–Maccoll theory for a normally incident supersonic flow over a cone is generalized to the case of obliquely incident flow as a basis to describe plasma mitigation mechanism. A plasma deflector generated by an electric discharge is modeled and the flow

deflection by this deflector is formulated in Section 3. Numerical illustration of the plasma deflection effect is also presented in Section 3. Wind tunnel experimental results to demonstrate shock mitigation by a plasma deflector, generated by 60 Hz periodic arc discharge, are presented in Section 4. In Section 5, a summary of the work is given, and conclusion remarks are drawn.

GENERATION OF TAYLOR–MACCOLL THEORY

In the Case of Parallel Flow

A supersonic flow propagates parallel to the cone axis from the left toward a cone. In the steady state, a conic shock front signified by a step pressure jump is formed to separate the flow into regions 1 and 2 of distinct entropies as sketched in Figure 1 with $\theta' = 0$. In the figure, the cone is placed horizontally (along the z-axis); thus, the flow velocity $\mathbf{V}_1$ in region 1 is along the z (cone's) axis, i.e., $\mathbf{V}_1 = V_1\hat{\mathbf{a}}_z = V_1(\hat{\mathbf{a}}_R \cos\beta - \hat{\mathbf{a}}_\theta \sin\beta)$, where $\hat{\mathbf{a}}_R$ and $\hat{\mathbf{a}}_\theta$ are unit vectors in the radial and poloidal directions of the spherical coordinate system, the origin is at the tip of the cone. The flow has a Mach number M_1. The conic shock wave angle β is to be determined. In region 2 immediately behind the shock front, the flow has a deflection angle δ with Mach number M_2 and velocity $\mathbf{V}_2 = V_2[\hat{\mathbf{a}}_R \cos(\beta - \delta) - \hat{\mathbf{a}}_\theta \sin(\beta - \delta)]$.

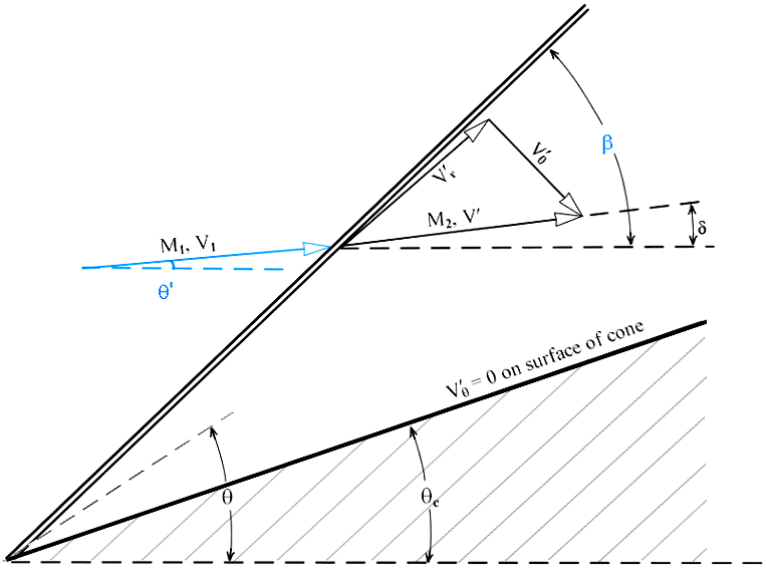


Figure 1: Geometric relations of the supersonic flow velocity at the discontinuity across the shock front of a cone.

Across a conic shock front (similar to across an oblique shock front), the continuity conditions of the flow at the discontinuity interface include: 1) the continuity of the flow, i.e., $\rho_1 V_1 \sin\beta = \rho_2 V_2 \sin(\beta - \delta)$ where ρ is the mass density of the flow; and 2) the preservation of the tangential component (i.e., $\hat{\mathbf{a}}_R$ component) of the flow velocity, i.e., $V_1 \cos\beta = V_2 \cos(\beta - \delta)$. The continuity, momentum, and energy equations show that the changes across the shock front are governed by the normal component of the free stream velocity, which is represented in terms of the normal component of the upstream Mach number $M_{n1} = M_1 \sin\beta$. The normal component of the downstream Mach number is obtained to be [1]

$$M_{n2}^2 = \frac{M_{n1}^2 + 2/(\gamma - 1)}{[2\gamma/(\gamma - 1)]M_{n1}^2 - 1} \quad (1)$$

Thus, the Mach number behind the oblique shock, M_2, can be find from M_{n2}, to be

$$M_2 = \frac{M_{n2}}{\sin(\beta - \delta)} \tag{2}$$

With the aid of (1) and (2), the continuity conditions of the flow are combined to relate the shock wave angle β and the deflection angle δ through a *δ–β–M* relation [1] [22]:

$$\tan\delta = 2\cot\beta \frac{M_1^2\sin^2\beta - 1}{M_1^2(\gamma + \cos2\beta) + 2} \tag{3}$$

where γ =1.4 is usually adopted. This relation specifies δ as a unique function of M_1 and β.

In the Case of Obliquely Incident Flow

Taylor–Maccoll theory is generalized to analyze a deflected supersonic flow over a cone by approximating curve shock front to be piecewise oblique shock front. The incoming flow from the left is now to propagate at a constant angle θ′ with respect to the axis of the cone as sketched in Figure 1, in which the oblique shock front represents a local approximation of a curve shock.

δ–β–M Relation (3) generalized to the Situation of θ′≠0

The relevant parameters in the equations, governed by the normal component of the free-stream velocity, are $M_{n1} = M_1\sin(\beta - \theta')$ and $M_{n2} = M_2\sin(\beta - \delta)$. Letting $\beta' = (\beta - \theta')$ and $\delta' = (\delta - \theta')$, these two relations become $M_{n1} = M_1\sin\beta'$ and $M_{n2} = M_2\sin(\beta' - \delta')$, which are the same mathematical forms as those in the θ′ = 0 case. In essence, this is to rotate the z axis counterclockwise by an angle θ′. Therefore, in the case of θ′ ≠ 0, the *δ–β–M* relation is extended to the *δ′–β′–M* relation [17] [22], which is

$$\tan\delta' = 2\cot\beta' \frac{M_1^2\sin^2\beta' - 1}{M_1^2(\gamma + \cos2\beta') + 2} \tag{4}$$

The Generalized Taylor–Maccoll Equation for Oblique Conical Flows

Equation 10.15 of Anderson book [1] for (β, δ) is generalized for (β′, δ′) to be

$$0.2\,(1 - G^2 - G'^2)(2G + G'\cot\theta + G'') - G'^2(G + G'') = 0 \tag{5}$$

where $G = V_{R2}/V_{2max} = (5/M_2^2 + 1)^{-1/2}\cos(\beta' - \delta')$, $G' = dG/d\theta$, $G'' = d^2G/d\theta^2$, and γ = 1.4 is assumed.

The boundary conditions of (5), at the poloidal angle θ = β, are given by

$$G(\beta) = f(M_2)\cos(\beta - \delta) = f(M_2)\cos(\beta' - \delta')$$

and (6)

$$G'(\beta) = -f(M_2)\sin(\beta - \delta) = -f(M_2)\sin(\beta' - \delta')$$

where δ′ is determined by (4); and $f(M_2) = V_2/V_{2max} = (5/M_2^2 + 1)^{-1/2}$, $M_2 = M_{n2}/\sin(\beta' - \delta')$, $M_{n2} = \{[(M_1\sin\beta')^2 + 5]/[7(M_1\sin\beta')^2 - 1]\}^{1/2}$. Thus, G(θ; β) and G′ (θ; β) can be evaluated for a given M_1 and β. If β represents the wave angle of the shock on a θ half-angle cone, an additional boundary condition that the normal component of the flow velocity on the cone surface is zero, i.e., G′ (θ; β) = 0, must be imposed.

Equation (5) can be solved for $G(\theta_c;\ \beta_c)$, where θ_c and β_c are the half-cone angle and the wave angle of the shock on the cone, via a direct or an inverse approach. The direct numerical approach is to continuously adjust the boundary conditions by varying β until $G'(\theta_c;\ \beta_c) = 0$ with a proper boundary angle $\beta = \beta_c$. From this, the wave angle β_c of the shock on a θ_c half-angle cone is determined.

On the other hand, it makes the calculation easy by employing an inverse approach; a given shock wave will be assumed and a specific cone that supports the given shock will be calculated. That is setting $\beta = \beta'_c$, a given shock wave angle β'_c, in (6) to solve (5) for $G(\theta;\ \beta'_c)$ and $G'(\theta;\ \beta'_c)$ until $G'(\theta = \theta'_c;\ \beta'_c) = 0$. Thus, a plot of β'_c verse θ'_c can be obtained; from which $(\theta_c;\ \beta_c)$ is determined. The effect of a localized plasma deflector on the shock wave is then inferred from changes in the deflection angle θ′ and in the Mach number M_1 of the flow, where θ′ and M_1 vary with r, the radial coordinate with respect to the z-axis.

At a fixed M_1, the deflection angle δ and the shock wave angle β, in the case of θ′ = 0, increase only with the half-cone angle θ_c [1]. This is illustrated in Figures 2(a) and (b). As the cone angle exceeds a critical value, i.e., $\theta_c > \theta_{cm}$, the solution of (5) cannot meet the boundary condition that the normal component of the flow velocity on the cone surface is zero anymore. Thus, the shock will become detached, and the oblique shock becomes a curve shock, as shown in Figure 2(c).

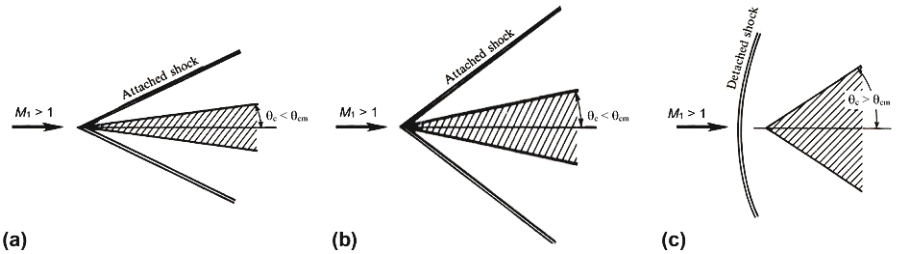


Figure 2(a) Attached oblique shock wave of a cone with $\theta_c < \theta_{cm}$; (b) increased shock angle with the increase of the cone angle; (c) changed to a detached curve shock as $\theta_c > \theta_{cm}$ [23].

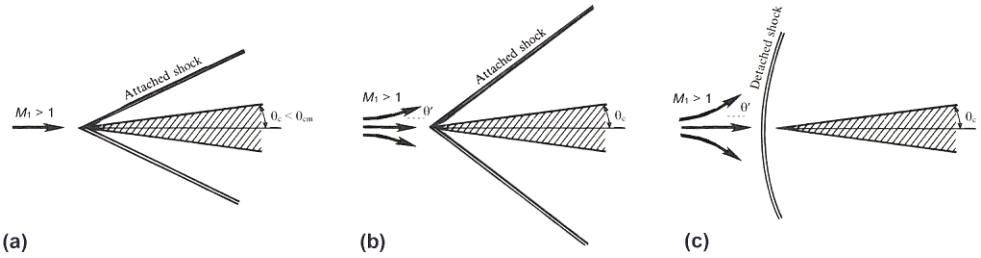


Figure 3(a) A baseline shock wave on a cone with $\theta_c < \theta_{cm}$; it is modified by the degree of the incoming flow deflection: (b) increase of the shock angle as the deflection angle $\theta' < \theta'_m$ and (c) becoming a detached curve shock as $\theta' > \theta'_m$ [23].

However, in the case of $\theta' \neq 0$, Eq. (4) indicates that the deflection angle δ and the shock wave angle β increase with the half-cone angle θ_c as well as with the deflection angle θ′ of the incoming flow.

It suggests that the shock wave angle of a fixed cone can be increased by introducing a symmetric deflection on the incoming flow, and further increase of the deflection can even modify the attached oblique shock to a detached curve shock. The impact of the flow deflection on the shock wave modification is illustrated in Figure 3, showing in sequence the envisioned shock wave changes with the increase of the flow deflection [23]. Therefore, if a plasma generated in front of the cone tip can effectively deflect the incoming flow symmetrically, it can mitigate shock wave impact by increasing the shock wave angle and changing oblique shock into detached curve shock. A significant deflection of the incoming flow may even impede the shock wave formation.

IMITATION AND ANALYSIS OF PLASMA DEFLECTOR

In Figure 1, the incoming airflow is deflected before reaching the baseline shock front of a cone. Thus, the plasma deflector must be generated in the upstream region of the shock front. In the following analysis, a plasma deflector is modelled in the form of a symmetrically distributed plasma in front of the baseline shock [22]-[26]; its impact on shock formation is analyzed.

Plasma Deflector

This plasma deflector is introduced at a location in front of a (cone-shaped) wind tunnel model by an on-board electrical discharge, which is triggered by a negative voltage applied between the grounded body of the cone and the tip of the cone located at z = 0, which is insulated from the body. A sharp tip helps to enhance the electric field intensity in the region in front of the tip and move the gas breakdown and discharge upstream. Using the planar projection of the model as a two-dimensional model, the equipotential lines between the two electrodes, with the central electrode biased negatively, are evaluated numerically by using a Poisson solver. The result is presented in Figure 4(a), in which the distribution of the electric field that is perpendicular to the equipotential line is also indicated. As shown, though the electric field intensity decreases with distance from the tip, the applied electric field can extend to a relatively large region upstream of the baseline shock front. This local field continuously accelerates electrons of the electric discharge in the upstream region. While moving upstream, electrons collide with the incoming flow to deflect it. The transverse momentum perturbation of the neutral flow is distributed symmetrically in the opposite direction to be net zero.

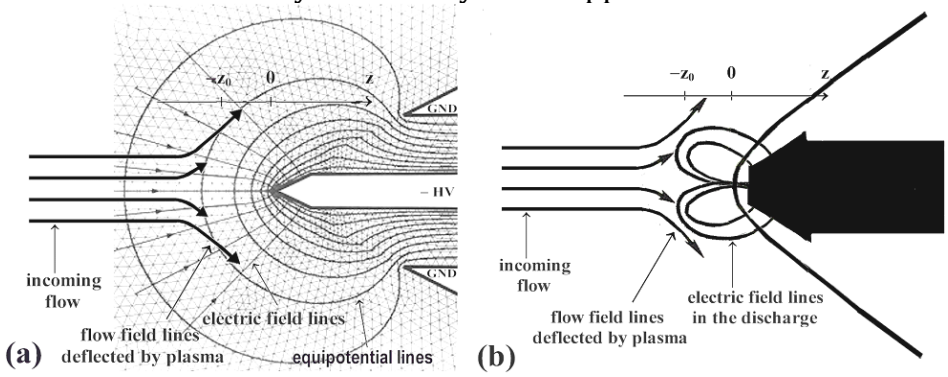


Figure 4 (a) Distributions of the equipotential line and electric field between two electrodes of a two-dimensional model and (b) imitation showing the envisioned electric field distribution supporting the discharge and the deflection of the incoming flow by the discharge-produced plasma [23].

An imitated figure to illustrate the flow deflection is presented in Figure 4(b), in which the electric field distribution is modeled to be $\mathbf{E}(r,z) \cong -(A_0/R^2)(z\hat{z} + r\hat{r})$, where (r, z) are the cylindrical coordinates, A_0 is proportional to the applied voltage and $R = (z^2 + r^2)^{1/2}$ is the distance of the field point away from the tip. Although the electron mass is much smaller than the ion mass, it is mainly the electrons, that move faster and collide the incoming flow much more frequently than ions, deflect the incoming flow. The net transverse momentum change of the deflected flow is zero, so the degree of deflection is not constrained by the conservation of transverse momentum.

We now consider that a uniform airflow from left to right with a velocity $\mathbf{V}_{10} = V_{10}\hat{z}$ encounters this plasma deflector at $z = -z_0$, as demonstrated in Figure 4(b). Electrons in the discharge interact with the airflow through elastic electron–neutral collisions. On the other hand, the ion–neutral interaction is more complicate. It involves both elastic and charge transfer inelastic collisions.

The electron density distribution of the plasma deflector is first determined through the spatial distribution of the ionization frequency $\nu_i \sim \varepsilon^{5.3}\nu_a$, where $\varepsilon = E/E_{cr}$, E_{cr} is the air breakdown threshold field, and ν_a is the electron-neutral attachment rate. Thus, $n_e(\xi) = n_0\exp[(\nu_i - \nu_a)t_0] = n_{e0}\exp\{-\eta[1-(1+\xi^2)^{-2.65}]\}$, where $\xi = r/z_0$, t_0 is the transient period for the plasma density to build up, $n_{e0} = n_e(0) = n_0\exp[(\nu_{i0} - \nu_a)t_0]$, $\nu_{i0} = \nu_i(\xi=0)$, $\eta = \nu_{i0}t_0$, and $\eta = 0.85$ will be assumed. The two electric field components in the interaction region at $z = -z_0$ are represented approximately by $E_z = E_0/(1+\xi^2)$ and $E_r = -E_0\xi/(1+\xi^2)$, where $E_0 = A_0/z_0$.

Flow Deflection

The momentum equations for the three fluids: electrons, positive ions, and neutral molecules, in a weakly ionized plasma in the presence of an imposed electric field are:

$$m_e\frac{d(n_e\mathbf{v}_e)}{dt} = -n_e m_e \nu_{en}(\mathbf{v}_e - \mathbf{V}_1) + n_e m_e \nu_{ei}(\mathbf{v}_i - \mathbf{v}_e) - en_e\mathbf{E} \quad (7)$$

$$m_i\frac{d(n_i\mathbf{v}_i)}{dt} = -n_i m_i \nu_{in}(\mathbf{v}_i - \mathbf{V}_1) - n_i m_i \nu_c(\mathbf{v}_i - \mathbf{V}_{10}) - n_e m_e \nu_{ei}(\mathbf{v}_i - \mathbf{v}_e) + en_i\mathbf{E} \quad (8)$$

$$m_n\frac{d(n_n\mathbf{V}_1)}{dt} = n_e m_e \nu_{en}(\mathbf{v}_e - \mathbf{V}_1) + n_i m_i \nu_{in}(\mathbf{v}_i - \mathbf{V}_1) + n_i m_i \nu_c(\mathbf{v}_i - \mathbf{V}_{10}) \quad (9)$$

where ν_c ($> \nu_{in}$) is the ion–neutral charge transfer collision frequency, which is dominated by charge transfer between the same type particles, e.g., the charge transfer cross-section between N_2^+ and N_2 in the relevant energy regime is larger than 3×10^{-19} m^2. After charge transfer, neutral particle converts to an ion which moves at the neutral's original velocity $\mathbf{V}_{10}$; and the ion converts to a neutral moving at ion's original velocity $\mathbf{v}_{i0}$. Since the ion's velocity is low, the converted neutrals form a subsonic flow, which will not contribute to the shock wave formation. On the other hand, the converted ions form a supersonic flow; but this ion flow is collected by the cathode as the current flow and heat generator. In essence, it weakens the incoming flow for the shock wave formation. Therefore, each of the ion and neutral fluids can be decomposed into two components, i.e., $n_i\mathbf{v}_i = n_{i1}\mathbf{v}_i^{(1)} + n_{i2}\mathbf{v}_i^{(2)}$ and $n_n\mathbf{V}_1 = n_{n1}\mathbf{V}_1^{(1)} + n_{n2}\mathbf{V}_1^{(2)}$, where n_{i1} and n_{i2} are the ion densities generated by the electric discharge and by the charge exchange conversion, respectively; n_{n1} and n_{n2} are the neutral density of the incoming flow and the

neutral density converted from the ions, respectively; thus $dn_{i2}/dt = dn_{n2}/dt = \nu_c n_{i1}$; and $v_i^{(1)} \sim v_{i0}, v_i^{(2)} \sim V_{10}, V_1^{(1)} \sim V_{10}$, and $V_1^{(2)} \sim v_{i0}$. In other words, the one with superscript 1 is related to shock formation, and the other, with superscript 2, is not related to shock formation. $n_{n2} << n_{n1}$ because the interaction region (plasma layer) is very narrow. To simplify the analysis, the inertial terms on the left-hand side and the electron–ion collision terms (proportional to ν_{ei} and ν_{ie}) on the right hand side of (7) and (8) are neglected; the approximated (7) and (8) yield $n_e m_e \nu_{en}\left(\mathbf{v}_e - \mathbf{V}_1^{(1)}\right) \cong -en_e\mathbf{E}$ and $n_{i1} m_i \nu_{in}\left(\mathbf{v}_i^{(1)} - \mathbf{V}_1^{(1)}\right) \cong [\nu_{in}/(\nu_{in} + \nu_c)]\, n_{i1}(e\mathbf{E} - m_i \nu_c \mathbf{V}_1^{(1)})$, which reduce (9) to be

$$\frac{d\mathbf{V}_1^{(1)}}{dt} = -\frac{\nu_c}{\nu_{in} + \nu_c}\frac{n_e}{n_n}\frac{e\mathbf{E}}{m_n} - \frac{n_{i1}}{n_n}\nu_c\left(\mathbf{V}_{10} + \frac{\nu_{in}}{\nu_{in} + \nu_c}\mathbf{V}_1^{(1)}\right) \quad (10)$$

where $n_{i1} \cong n_e$ is assumed. In (10), the pressure gradient term is neglected because the density and temperature of the incoming airflow do not change much in passing through the plasma deflector. We now integrate (10) over a transit period $t_n = z_0/V_{10}$, the time for the airflow to pass through the plasma deflector of length z_0. We obtain

$$\mathbf{V}_1^{(1)}(r, t_n) \cong V_{10}\hat{z} - V_{10}\exp\{-\eta[1 - (1 + \xi^2)^{-2.65}]\}[\alpha_n(1 + \xi^2)^{-1}(\hat{z} - \xi\hat{r}) + \beta_n\hat{z}] \quad (11)$$

where $\alpha_n = [\nu_c/(\nu_{in} + \nu_c)]\,(eE_0 t_n/V_{10}m_n)(n_{e0}/n_n)$ and $\beta_n = (n_{e0}/n_n)\,(\nu_c t_n)\,[1 + \nu_{in}/(\nu_{in} + \nu_c)]$. The deflected flow has a deflection angle θ' and Mach number M_1, which are obtained from (11) to be $\theta'(r) = \tan^{-1}[V_{1r}(r)/V_{1z}(r)]$ and $M_1(r) = \{[V_{1r}^2(r) + V_{1z}^2(r)]^{1/2}/V_{10}\}M_{10}$, where M_{10} is the Mach number of the unperturbed flow.

Numerical Analysis

In the numerical calculations, the parameters of the incoming flow are: $M_{10} = 2.5$, $n_n \sim 10^{25}\ m^{-3}$ (i.e., $P_1 = 0.175$ atm and $T_1 = 135$ K), $V_{10} = 570$ m/s, and $\nu_c \cong 2\nu_{in} \cong 2.16\times10^9\ s^{-1}$, which are comparable with the experiments to be presented in the next section.

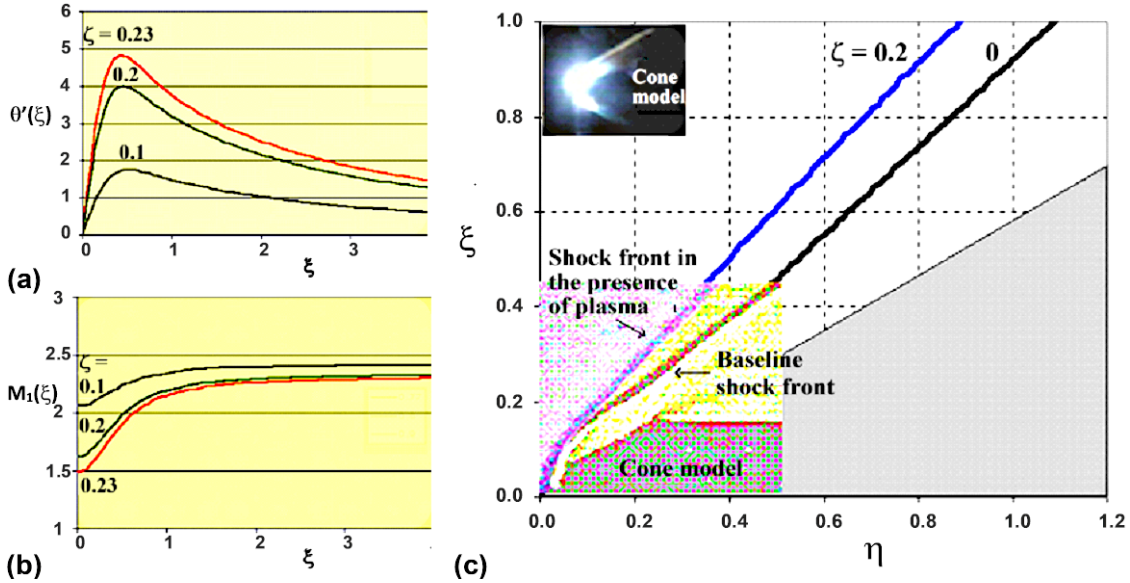


Figure 5(a) θ′ (ξ), the deflection angle, and (b) $M_1(\xi)$, the Mach number, of an incoming flow after being scattered by a plasma spike; (c) attached shocks in a supersonic flow over a 60⁰ cone (represented by the shadow region) for two cases, ζ = 0 (no discharge) and ζ = 0.2 (corresponding to an intense discharge), where $\xi = r/z_0$ and $\eta = z/z_0$. The line labeled ζ = 0 represents the baseline shock front. A superimposed shadowgraph of a baseline shock front and a plasma mitigated shock front is inserted at left lower corner for comparison with the numerical results. The insert at left upper corner shows the plasma deflector [23].

The deflection angle θ′(r) and the Mach number $M_1(r)$ of the deflected flow vary with the intensity of the discharge (depending on the applied electric field intensity and gauged by the maximum electron density n_{e0}). Set $E_0 \sim 10^6$ V/m and $t_n = 0.88\times10^{-5}$ s (i.e., $z_0 = 5$ mm), the parameters α_n and β_n in (11) become $\alpha_n = 0.334\times10^{-20}\, n_{e0}$ and $\beta_n = 0.253\times10^{-20}\, n_{e0}$. Let $n_{e0} = 3\times10^{20}\,\zeta\ m^{-3}$, where ζ is a variable parameter to weigh the discharge situation, so that $\alpha_n = \zeta$ and $\beta_n = 0.76\zeta$. The two functions θ′(r) and $M_1(r)$ are plotted in Figures 5(a) and (b) for the parameter ζ = 0.23, 0.2, and 0.1.

Using these results for each ζ (i.e., n_0) as the parameters at the shock front location, the corresponding oblique angle $\beta_c(r) = \beta'_c + \theta'$ of the shock front can be determined by solving (5) iteratively to meet the condition that the normal component of the flow velocity on the cone surface $G'(\theta_c;\beta_c) = 0$. Thus, the position of the shock front can be determined by the trajectory equation:

$$\frac{dz}{dr} = \cot\beta_c = \cot\left(\beta'_c + \theta'\right) \tag{12}$$

The result in the case of ζ = 0.2 (corresponding to a relatively intense discharge) is presented in Figure 5(c), in which the baseline shock front, having a shock angle $\beta_0 = 42.6^o$ (for $\theta_c = 30^o$), is also presented for comparison. As shown, the shock angle is increased to 46^o by the plasma spike; agreeing well with the experimental result which is inserted at the left lower corner of the same figure for comparison. In this case, the peak electron density of the plasma deflector used in the numerical calculation is $n_{e0} = 6\times10^{19}\ m^{-3}$, which agrees with that

produced by the on-board diffused arc discharge, shown in the insert at the left upper corner of the same figure.

For each ζ, a $\beta_c(\xi)$ distribution is determined. In terms of the determined $\beta_c(\xi)$ and δ for β' and δ' in (4), one can obtain an equivalent Mach number distribution $M_{1eq}(\xi)$, which is found to agree with the corresponding $M_1(\xi)$, presented in Figure 5(b) and is smaller than M_{10}, as expected.

Experimental study on the feasibility of a plasma deflector for shock wave mitigation is presented next.

EXPERIMENT

Experiments were conducted in the test section, with a 0.38 m × 0.38 m cross section of a supersonic blow-down wind tunnel. It is aimed at confirming the theoretical study of shock wave mitigation by a plasma deflector, presented in Secs. 2 and 3. The upstream airflow had a flow speed v = 570 m/s, temperature T_1 = 135 K, and a pressure P_1 = 0.175 atm.

Wind Tunnel Model and Electric Discharge

Implement a plasma torch module [27] in a truncated-cone-shape wind tunnel model for on-board periodic electric discharges. This truncated-cone body is connected to a cylindrical body attached to a holder. The torch module consists of a sharpened solid tungsten rod of a diameter d = 2.4 mm, as the central electrode, and a ceramic insulator which holds the tungsten rod in place concentrically with the truncated-cone body, as the outer electrode, to form the electrode pair for the discharge. The sharpened solid tungsten rod together with the ceramic insulator also mean to fill in the truncation of the cone, which recovers the model to a cone. A schematic of the model is presented in Figure 6(a). The truncated 60^0 cone has a frontal diameter D = 11.1 mm and a height L = 12.7 mm. The cylindrical base of the cone has a diameter D_b = 25.4 mm.

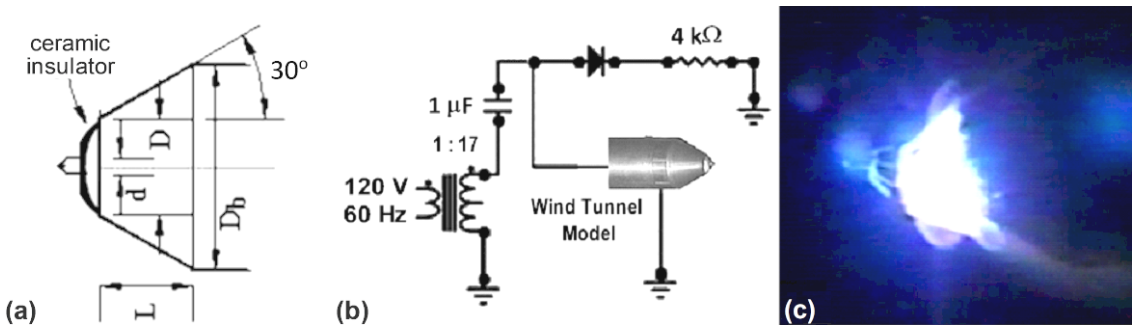


Figure 6(a) Schematic of the wind tunnel model implemented with electric discharge electrodes for plasma generation, (b) the circuit for 60 Hz periodic electric discharge, and (c) a photo of the plasma deflector generated by arc discharges in a supersonic flow.

The gap between the tungsten rod and the inner wall at the front of the truncated-cone body is 3.5 mm. The breakdown voltage is provided by a power supply sustaining 60 Hz periodic electric discharge. The nose of the model, shown in Figure 6(a), is a cone-shaped ceramic insulator with a short protruding spike, which replaces the truncated part of the cone. The distance from the tip to the edge of the truncated-cone surface is about 5 mm. The 60 Hz power

supply for periodic discharge operation is shown in Figure 6(b). During one of the two half cycles when the diode is forward biased, the capacitor is charged so the voltage across the electrodes is low and there is no discharge. During the other half cycle, the diode has a reverse bias. The charged capacitor increases the voltage across the electrodes and breakdown occurs. The discharge normally initiates in the region near the tip electrode where the applied electric field concentrates due to the cylindrical geometry. Therefore, it prefers the tip electrode to be negative so that the electrons can be pushed to the upstream region. The discharge produces spray-like plasma, shown in Figure 6(c), to act as a spatially distributed deflector, which deflected the incoming flow. Indeed, plasma effect on the shock wave structure has been observed only when the tip of the model is designated as the cathode.

The output voltage of the power supply has a peak of about 4.5 kV, exceeding the 4 kV (for 5-mm gap) required for avalanche breakdown. The electric field intensity near the tip exceeds 1 MV/m before breakdown occurs. It reduces to a level less than 100 kV/m as the discharge current reaches the peak. The peak and average power of the discharge are about 1.2 kW and 100 W, respectively. The maximum electron density of the discharge exceeds 10^{19} m^{-3}.

Optical Diagnostics

Shadowgraph method was used to optically diagnose the flowfield around the spike and nose of the cone. A black and white (BW) charge coupled device (CCD) camera, with a frame rate of 30 frames per second and exposure time of 1/60 s (which is slightly less than four times of each discharge period), was used to directly record the shadowgraph images of the flow dynamics. A video (color CCD) camera as the corresponding one to the BW CCD camera was used to record the spatial distribution and temporal evolution of the plasma glow with the same frame rate and exposure time. The video graph recorded in each frame is an integrated result over the exposure time, and thus the temporal variation of the shock wave structure and plasma glow during a single discharge period cannot be recorded directly.

Plasma Glow

Although a 60 Hz power supply is used, the synchronization between the electric discharge and the exposure cycle of the camera is not controllable. Moreover, the electric discharge is not exactly periodic because the starting time of each discharge varies, and the discharge glow has temporal resolution up to 100 msec. Thus, the plasma plume image varies with the variation of the overlapping duration between the discharge and the camera exposure period. A neutral density filter was applied to the CCD camera for reducing the airglow intensity of the discharge entering the camera. It works to reduce the integral effect of a finite exposure time on showing the temporal variation of the discharge. Growth and decay of the plasma glow in the electric discharge can then be revealed by extracting frames from a continuous video graph of the plasma plume. A sequence of 6 assembled video graphs.

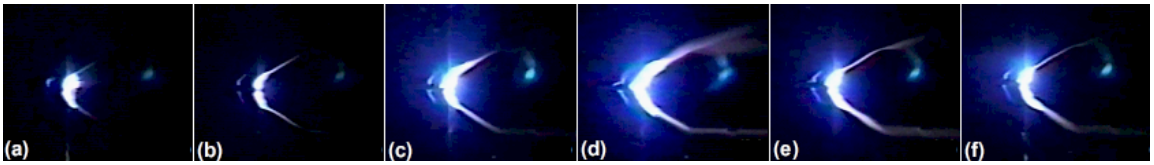


Figure 7An assembled time sequence of six video graphs showing the growth and decay of the plasma glow during one discharge period in the middle of a wind tunnel run at Mach 2.5.

showing the growth and decay of the plasma plume in the electric discharge, with a symmetric spatial distribution with respect to the axis of a cone, are presented in Figure 7. In the video graphs, the flow is from left to right.

The Shadow Imaging System

A schematic of the optical setup for simultaneous Shadow and Plasma Glow/Afterglow video imaging is shown in Figure 8. An incandescent lamp with beam-forming optics and filters, was used for the present reported observations. A parabolic mirror, of diameter 0.3 m and focal length of 3.7 m, collimated the divergent beam from the (point) light source before it passed through the wind tunnel test section windows. On the other side of the wind tunnel, an image forming optics, consisting of a lens and a B&W high resolution CCD camera, was used to obtain the Shadow images. The Shadow images were projected directly on the CCD area, avoiding the use of projection screens, and recorded at a rate of 30 frames/sec with an exposure time of 1/60 sec. The image magnification could be modified in the range 0.1-0.5 mm/pixel by camera positioning along the optical axis. Neutral density filters were used to cut down light intensity coming from the flow itself, instigated by the discharge. The images extracted from videos recording the shadowgraph images of the flow can provide the correlation between the strength of the plasma deflector and the degree of the shock structure modification through the background brightness of the shadowgraph images.

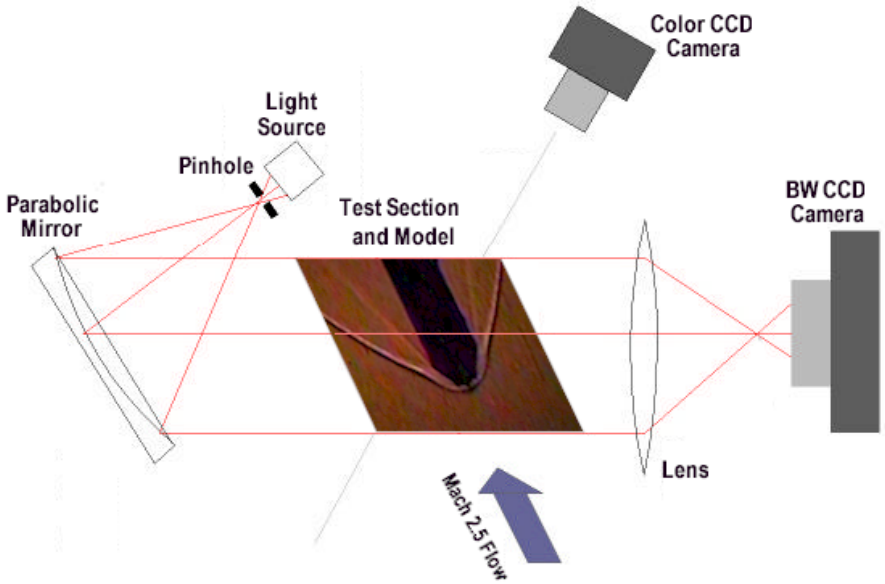


Figure 8.Schematic of an optical setup.

The synchronization between shadow and plasma glow recorded images was realized by post-processing of the corresponding images (based on the discharge glow that has temporal resolution of less than 100 msec). Tracking of video frames showed that the frame synchronization error between cameras during one-run duration (100-300 frames) was less than half frame that was less than 1/120 sec. The images extracted from two videos can provide the correlation between the strength of the plasma deflector and the degree of the shock structure modification; and any consistent relationships appearing in the correlation are useful to determine the plasma conditions for achieving significant plasma effect on the shock wave.

Experimental Results

The spray-like plasma, generated by the electric discharge, acted as a spatially distributed plasma deflector, which was used to deflect the incoming flow. This deflector increased its size and intensity from a low level to the maximum and then decayed to a low level, resembled in Figure 7. The modification effect shown in a shadowgraph is expected to depend on the density, volume, spatial distribution, and location of the plasma deflector produced by the electric discharge, as well as the actual interacting time between flow and plasma deflector in the exposure cycle of the CCD. Although the temporal variation of the shock wave structure during a single discharge period could not be recorded directly; the desired information regarding the temporal variation of the flowfield during the discharge could be extracted from the continuous video graph of the flow, using the background brightness of the shadowgraph as a reference. A set of 6 shadowgraphs, presented in Figure 9, resembles the responses of the incoming flow to the growth and decay of the plasma deflector in one discharge cycle. In this and other shadowgraphs presented later, the flow is from left to right. The growth of the plasma deflector is manifested by the intensifying of the background brightness in the shadowgraphs.

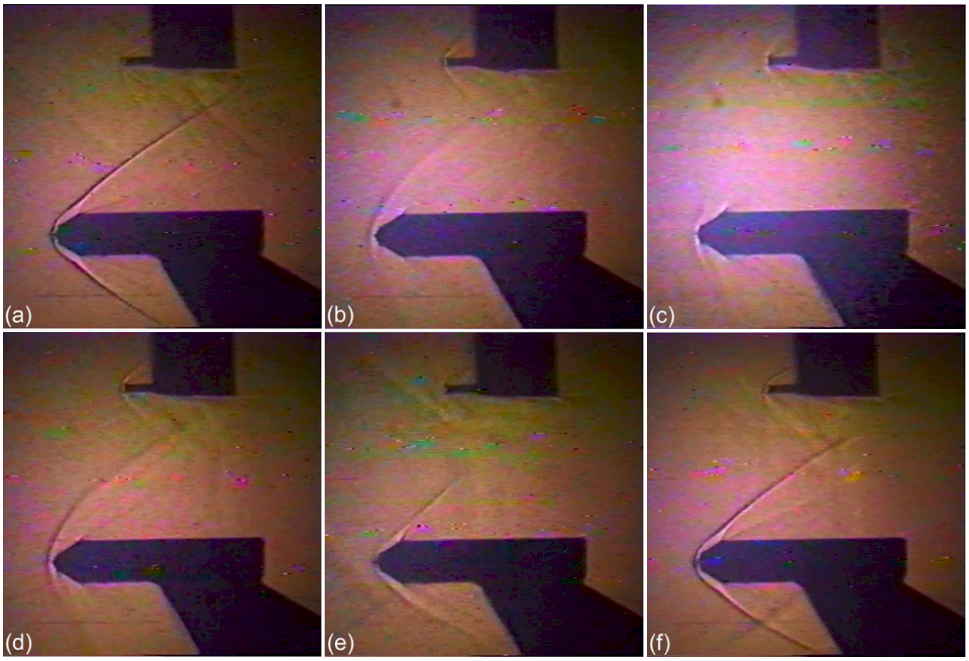


Figure 9 An assembled time sequence of six shadowgraphs (a)-(f) to resemble the flow response to the plasma deflector during one discharge period in the middle of a wind tunnel run at Mach 2.5.

First, shadowgraph shown in Figure 9(a) is in the case that the discharge just starts Therefore, the shadowgraph is darker (absence of background light from the plasma) and is like the baseline one. The next two presented in Figures 9(b) and (c) correspond to the situation that the discharge is intensifying to reach the peak. As shown in Figure 9(b), the intensified discharge first moves the baseline shock front upstream to become a detached curve shock front. As the plasma deflector is further intensified to reach the strongest level, its modification effect on the shock structure also reaches the maximum. The curve shock front in Figure 9(c) is much diffused, with larger curve angle and weaker aspect. As the intensity of plasma deflector decreases from the maximum level, the shock front also recovers toward to the baseline in the sequence of Figures 9(d) to (f). A well-defined curve shock front reappears in Figure 9(d). It

moves downstream to become an attached oblique shock (in fact, it is a conical shock in 3-D) as shown in Figure 9(e), but the shock front appears to be weaker than that of the baseline. The baseline shock front reappears in Figure 9(f) as the discharge is reduced to low level again. The recovery of the baseline shock front presented in Figure 9(f) indicates the steady of the incoming flow during the discharge cycle. These observations on unsteady shock motion and structure change are typical of the experimental results recorded in the video tapes.

The pronounced influence of plasma on the shock structure is demonstrated by the result shown in Figure 9(c). A comparison of Figures 9(c) and (a) clearly observes a transformation of the shock from a well-defined attached shock into a diffused and highly curved shock structure having a diminished aspect. This modification is an indication of shock wave being weakened by this air plasma mitigator. Applying non-thermal plasma to mitigate shock wave [17] [20] is an ultimately desirable result that reduces wave drags and shock noise at supersonic speeds; significantly improving supersonic flight.

Tracking of video frames from two cameras during one-run duration (100-300 frames), the correlation between the mitigation of the shock and the plasma deflector is further revealed, as shown in Figure 10. A time sequence of four shadowgraphs (a) to (d) is found to correspond to the glow images of the plasma deflector (e) to (h), extracted from frames recorded in the middle of a wind tunnel run at Mach 2.5.

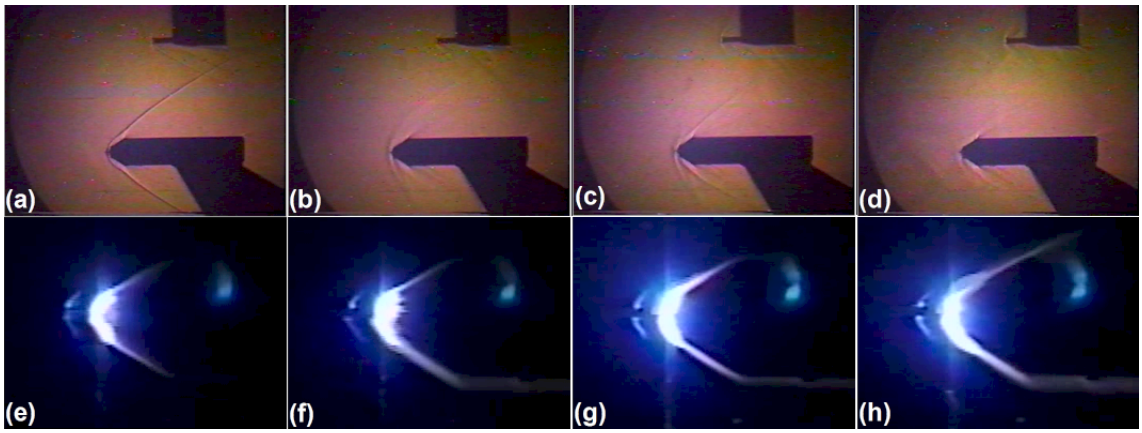


Figure 10 An assembled time sequence of four shadowgraphs (a)-(d) to represent the flow response to the plasma deflector (e)-(h) during one discharge period in the middle of a wind tunnel run at Mach 2.5.

First, the shadowgraph shown in Figure 10(a) is in the situation that the discharge, shown in Figure 10(e), is in the early stage. The shadowgraph still records the baseline shock. As the plasma glow is intensifying as shown in Figures 10(f) and (g), the corresponding shadowgraphs presented in Figures 10(b) and (c) also reveal enhancing shock mitigation. The baseline shock front is first split into two (Figure 10(b)), with a new one located upstream; then it evolves to a curved new one, weaker and more diffusive, as shown in Figure 10(c). As the plasma deflector is intensified to the peak, as shown in Figure 10(h), its modification effect on the shock structure also reaches the maximum. As shown in Figure 10(d), the curved new one disappears, and the remaining structure becomes diffusive in the form of expansion waves.

Three snapshots of the flow during a wind tunnel run are chosen to further demonstrate plasma mitigation of shock wave. Those are superimposed into one presented in Figure 11a. The insert in Figure 11 exemplifies that plasma generated by the discharge has a distribution spreading around the cone model. Clearly, plasma causes the shock front to move upstream with increasing standoff distance from the model, to become more and more diffused, and to increasing shock angle in the process. A shock-free state is also observed as the discharge is further intensified. This is demonstrated in Figure 11(b). Using non-thermal plasma to eliminate shock has a significant impact on the supersonic flight; it minimizes wave drags and shock noise while flying at supersonic speeds; thus, it reduces fuel consumption and likely suspends the restriction of commercial flight over land.

Based on the measured peak and average discharge power, the upper bound of the peak and average temperature enhancements are estimated to be $\Delta T_{peak} \cong 26$ K (for $P_{in}|_{peak} = 1.2$ kW) and $\Delta T_{ave} \cong 2.2$ K (for $P_{in}|_{average} = 100$ W). The peak temperature perturbation is less than 10% of the unperturbed, 285 K, in the region behind the shock, and less than 20% of the upstream gas temperature of 135 K; and the average temperature perturbation is less than 1 and 2%, respectively. Thus, the heating could at most increase the sound speed and decrease the Mach number by 5%. These changes were too small to introduce any significant thermal effects.

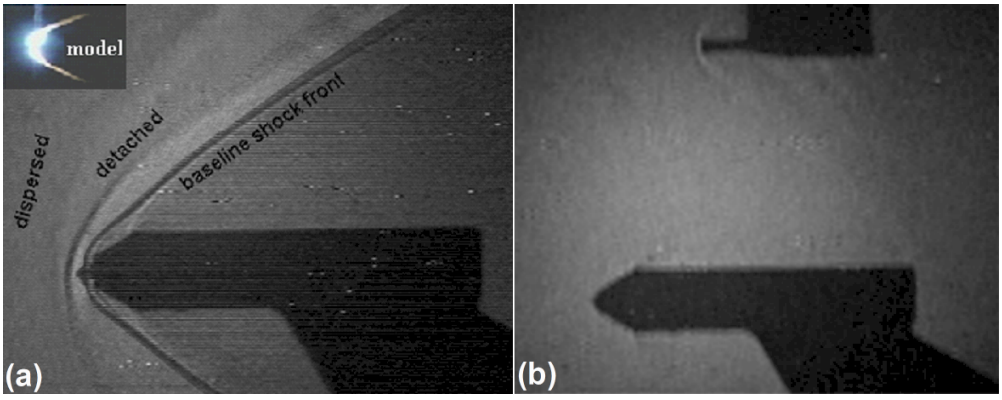


Figure 11(a) A superimposed shadowgraph showing the (attached) baseline shock front and two detached shock fronts modified by plasma with increasing discharge intensity; the insert shows the plume image of the plasma produced by the electrical discharge; (b) at the time when the discharge is around the peak and shock wave is eliminated.

SUMMARY AND CONCLUSIONS

A theory based on the deflection of the incoming flow by a symmetrically distributed plasma deflector in front of the shock as the process to modifying the shock wave structure has been formulated. Flow deflection increases the equivalent cone angle, which in turn increases the attached oblique shock wave angle. Moreover, when this equivalent cone angle exceeds a critical angle, the shock becomes a detached curve shock.

Wind tunnel experiments were conducted to explore the non-thermal plasma mitigation of the shock, studying the feasibility of the plasma deflection approach. A cone-shaped model was used as the shock generator and was facilitated with electrodes for on-board 60 Hz discharge to generate plasma in front of the model. The tip of the central electrode in the model was shaped to match the cone angle and to enhance the electric field intensity in the region in front of the tip. The central electrode was set as the cathode. This arrangement together with the

favorable electric field distribution made electron flow in the discharge much easier to pass through the shock front into the upstream (lower pressure) region before returning to the body of the model, set as the anode. As shown in Figure 7, the plasma glow of the discharge extends to the upstream region and has a symmetric distribution around the central electrode; under these conditions, the plasma deflector effectually deflect incoming flow to achieve shock wave mitigation.

As shown in the sequence of 6 shadowgraphs presented in Figure 9, the introduced plasma caused the shock front to increase angle and dispersion in its structure and standoff distance from the model, becoming detached curve shock.

The theoretical deflection model is analyzed numerically. As demonstrated in Figure 5(c), the numerical results are in good agreement with the experimental results that the plasma deflector increases the oblique shock wave angle. The experimental results presented in Figures 10 and 11 also demonstrate that the plasma deflector can indeed convert an attached oblique shock to a detached curve shock, as indicated by the theory. Figure 11(b) also demonstrates a shock-free state, an eventually desirable outcome of shock mitigation.

The wave drags and noise of the shock on the cone depends on the strength of the shock, which in turn depends on the Mach number of the flow as well as the shock wave structure. Numerical analysis shows that the effective Mach number $M_{1\mathrm{eq}}(\xi)$ of a deflected flow in the tip region of a shock generator is smaller than the unperturbed one (M_{10}). A decrease in the effective Mach number of the incoming flow in the tip region suggests that the plasma deflector reduce the wave drag of the shock on a supersonic aircraft.

Wind tunnel experiments show that a plasma deflector can indeed modify the shock structure, from an attached oblique shock to a detached curve shock, and even to become shock-free. The modified shock structure moving upstream and becoming diffusive, has lower wave drags and shock noise generated in the flow.

ACKNOWLEDGEMENTS

The author is grateful to Dr. D. Bivolaru for collaborative work. This work was supported in part by the Air Force Office of Scientific Research Grant AFOSR-FA9550-04-1-0352.

References

[1].Anderson, Jr., J.D., *Modern Compressible Flow*. 1990, McGraw-Hill, New York.

[2].Chang, P.K., *Separation of Flow*. 1970, Pergamon, Oxford.

[3].Batdorf, S.B., *Alleviation of the Sonic Boom by Thermal Means*. J. Aircraft, 1972. 9(2): p. 150-156.

[4].Levin, V.A. and L.V. Taranteva, *Supersonic Flow over Cone with Heat Release in the Neighborhood of the Apex*. Fluid Dynamics, 1993. 28(2): p. 244-247.

[5].Riggins, D., H.F. Nelson, and E. Johnson*, Blunt-Body Wave Drag Reduction Using Focused Energy Deposition*. AIAA Journal, 1999. 37(4): p. 460-464.

[6].Schülein, E. and A. Zheltovodov, *Effects of Steady Flow Heating by Arc Discharge Upstream of Non-slender Bodies*. Shock Waves, 2011. 21(4): p. 383-396. DOI: 10.1007/s00193-011-0307-1

[7].Markhotok, A., *A Mechanism of Wave Drag Reduction in the Thermal Energy Deposition Experiments*. Physics of Plasmas, 2015. 22(6): p. 063512. DOI: 10.1063/1.4922434

[8].Gordeev, V.P., A.V. Krasilnikov, V.I. Lagutin, and V.N. Otmennikov, *Plasma Technology for Reduction of Flying Vehicle Drag*. Fluid Dynamics, 1996. 31(2): p. 313-317.

[9].Baryshnikov, A.S., I.V. Basargin, E.V. Dubinina, and D.A. Fedotov, *Rearrangement of the Shock Wave Structure in a Decaying Discharge Plasma*. Technical Physics Letters, 1997. 23(4): p. 259-260.

[10].Kuo, S.P., I.M. Kalkhoran, D. Bivolaru, and L. Orlick, *Observation of Shock Wave Elimination by a Plasma in a Mach-2.5 Flow.* Physics of Plasmas, 2000. 7(5): p. 1345-1348.

[11].Kuo, S.P. and D. Bivolaru, *Plasma Effect on Shock Waves in a Supersonic Flow*. Physics of Plasmas, 2001. 8(7): p. 3258-3264.

[12].Appartaim, R., E.D. Mezonlin, and J.A. Johnson III, *Turbulence in Plasma-Induced Hypersonic Drag Reduction*. AIAA Journal, 2002. 40(10): p. 1979-1983.

[13].Bivolaru, D. and S.P. Kuo, *Observation of Supersonic Shock Wave Mitigation by Plasma Aero-Spike*. Physics of Plasmas, 2002. 9(2): p. 721-723.

[14].Bivolaru, D. and S.P. Kuo, *Aerodynamic Modification of Supersonic Flow around Truncated Cone using Pulsed Electrical Discharges*. *AIAA Journal*, 2005. 43(7): p. 1482-1489.

[15].Kuo, S.P. and D. Bivolaru, *The Similarity of Shock Waves Generated by a Cone-shaped Plasma and by a Solid Cone in a Supersonic Airflow*. Physics of Plasmas, 2007. 14(2): p. 023503 (1-5).

[16].Joussot, R. and V. Viviana Lago, *Experimental Investigation of the Properties of a Glow Discharge Used as Plasma Actuator Applied to Rarefied Supersonic Flow Control Around a Flat Plate*. IEEE Transactions on Dielectrics and Electrical Insulation, 2016. 23(2): p. 671 – 682. DOI: 10.1109/TDEI.2015.005327

[17]. Kuo, S.P., *Plasma Mitigation of Shock Wave: Experiments and Theory*. Shock Waves, 2007. 17(4): p. 225-239. Doi 10.1007/s00193-007-0112-z

[18].Sun, Q. , B.Q. Cheng, Y.H. Li, W.S. Kong, J. Li, Y.F. Zhu, and D. Jin*, Computational and Experimental Analysis of Mach 2 Air Flow Over a Blunt Body with Plasma Aerodynamic Actuation*. Science China Technological Sciences, 2013. 56(3): p. 795-802.

[19].Exton, R.J., R.J. Balla, B. Shirinzadeh, G.J. Brauckmann, G.C. Herring, W.C., Kelliher, J. Fugitt, C.J. Lazard, and K.V. Khodataev, *On-Board Projection of a Microwave Plasma Upstream of a Mach 6 Bow Shock*. Physics of Plasmas, 2001. 8(11): p. 5013-5017.

[20].Kuo, S.P., *Air plasma Mitigation of Shock Wave*. Advances in Aerospace Science and Technology, 2016. 1(2): p. 59-69. doi: 10.4236/aast.2016.12006.

[21].Brown, S.C., *Basic Data of Plasma Physics.* 2nd edition 1967, MIT Press, Cambridge.

[22].Kuo, S.P. and Steven S. Kuo, *A Physical Mechanism of Non-thermal Plasma Effect on Shock Wave*. Physics of Plasmas, 2005. 12(1): p. 012315(1-5).

[23].Kuo, S.P., *Shock wave mitigation by air plasma deflector*. Advances in Aerospace Science and Technology, 2018. 3(4): p. 71-88. Doi: 10.4236/aast.2018.34006.

[24].Kuo, S.P., *Conditions and a Physical Mechanism for Plasma Mitigation of Shock Wave in a Supersonic Flow*. Physica Scripta, 2004. 70(2-3): p. 161-165.

[25].Kuo, S.P., *Shock Wave Modification by a Plasma Spike: Experiment and Theory*. Physica Scripta, 2005. 71(5): p. 535-539.

[26].Kuo, S.P. and Steven S. Kuo, *Theoretical Study of Plasma Effect on a Conical Shock Wave*. Physics of Plasmas, 2006. 13(3): p. 033505 (1-6).

[27]. Kuo, S.P., E. Koretzky, and L. Orlick, *Methods and Apparatus for Generating a Plasma Torch*. United States Patent, 2001. US 6329628 B1.